







High power Raman second stokes generation in a methane filled hollow core fiber

ANN M. LANARI,^{1,*} HANS CHRISTIAN HANSEN MULVAD,¹ SEYED MOHAMMAD ABOKHAMIS MOUSAVI,¹  IAN A DAVIDSON,¹  QIANG FU,¹  PETER HORAK,¹  DAVID J RICHARDSON,² AND FRANCESCO POLETTI¹

¹Optoelectronics Research Centre, University of Southampton, Southampton, SO17 1BJ, UK

²Lumenity, Microsoft, Romsey, SO51 9DL, UK

*a.m.lanari@soton.ac.uk

Abstract: We demonstrate a multi-watt, picosecond pulse duration laser source by exploiting a cascaded Raman process to the second Stokes signal at a wavelength of 2.58 μm in a methane-filled Nested Anti-Resonant Nodeless fiber from a 1 μm disk laser source. A maximum average power of 2.89 W (14.45 μJ) is produced in a 160 cm length of custom-designed and in-house fabricated fiber filled with methane at a pressure of 2 bar. The impact of gas pressure and propagation distance on the second Stokes signal power are investigated experimentally. The experimental results are simulated by solving the Generalized Nonlinear Schrodinger Equation with the experiment carefully modelled by accounting for the impacts of pressure dependent gas-light interactions along the pressure gradient of the fiber. This work offers a laser source for a variety of applications as well as expanding the modelling space to methane filled fibers including pressure gradients, and nonlinear optical activity in the presence of infrared gas absorption.

Published by Optica Publishing Group under the terms of the [Creative Commons Attribution 4.0 License](https://creativecommons.org/licenses/by/4.0/). Further distribution of this work must maintain attribution to the author(s) and the published article's title, journal citation, and DOI.

1. Introduction

Mid-infrared (MIR) laser sources are required for several applications including: molecular spectral fingerprints, spectroscopy, micromachining, medicine, and free-space communications [1–7]. In recent years, Hollow Core fibers (HCF) have been shown to be an excellent medium to generate laser devices based on frequency up and down conversion from gas-light interactions [8–23]. The tight confinement of light to the core of the fiber, the high damage threshold from low glass-light overlap, and the low propagation losses [24] make Nested Anti-Resonant Nodeless fibers (NANF) a particularly appealing option for these types of interactions: the fiber can handle the coupling of high peak and average power pump sources while minimising the undesirable effects typically observed in glass-core fibers [25].

Raman cascades to mid-infrared wavelengths in gas-filled HCF are an appealing option for generating MIR sources [10,11,13,17–20,23,26]. Several Raman active gases have adequate gain and sufficiently large vibrational Raman shifts to reach the MIR from widely available 1 μm laser sources [27]. Hydrogen and deuterium offer vibrational shifts of 4155 cm^{-1} and 2987 cm^{-1} respectively [27] with high Raman gain but due to their anisotropic polarizability, they also exhibit rotational Raman scattering [28]. The excitation of rotational scattering can deplete the pump signal, reducing conversion efficiency to the desired vibrational Stokes wavelength [26]. The relatively small rotational Raman shifts in gases may broaden the pulse into a supercontinuum [18] particularly in the presence of nonlinear Kerr broadening [29]. Methane (CH_4) has a vibrational Raman shift (VRS) of $\sim 2916 \text{ cm}^{-1}$ and a Raman gain rivaled only by hydrogen but does not have rotational Raman activity due to its isotropic polarizability [28]. The large

vibrational shift, lack of rotational scattering, and high gain of methane make it an excellent candidate for achieving Raman cascades to the MIR and is why it is chosen for this work. To achieve MIR output from CH₄ using a 1 μm pump, a cascade to the second Stokes signal is required.

Some applications utilize or require picosecond pulse duration sources, taking advantage of the high peak powers and/or average powers available, [6,7] and the temporal characteristics of a Raman generated signal mirror that of its pump source [14]. The Raman dynamics of methane gas pumped with a picosecond pulse occur in the transient gain regime [30]. In the transient regime we can expect moderate Raman gain with a high degree of molecular coherency, as opposed to low gain in the spontaneous regime, and high gain but low molecular coherency in the steady state regime. In this work we generate a record-high average power 2.58 μm source in a CH₄ filled NANF with ~ 6 ps pulse duration.

2. Experiment

2.1. Fiber characteristics

We designed a custom HCF to provide low loss propagation windows at the wavelength of the laser pump available for our experiment, 1030 nm, the first Stokes wavelength, 1472 nm, and the second Stokes wavelength 2580 nm. A five element NANF is designed to support the Raman cascade to the second Stokes. An optimum thickness for the nested elements is determined to be 1.88 μm . The fiber is drawn in-house with a 40 μm core diameter, outer nested elements with a thickness of 1.87 μm , and inner nested elements with a thickness of 1.88 μm . A scanning electron microscope (SEM) image of the fiber is shown in the inset of Fig. 1. In this NANF design, the pump wavelength is in the fourth propagation window, the first Stokes wavelength is in the third propagation window, and the second Stokes wavelength is in the second propagation window.

A cutback measurement is performed to determine the propagation loss of the fiber. A Leukos Electro MIR4.8 supercontinuum source is coupled into a 251 m length of fiber and the spectrum is observed by both a Yokogawa AQ6370C Near Infrared (NIR) Optical Spectrum Analyzer (OSA), and Yokogawa AQ6376 MIR OSA to cover the full spectrum from 800 nm – 2800 nm. The fiber is then cut back to 10 m without altering the launch to determine a linear loss over the wavelengths observed by the two OSAs. During the cutback, the fiber is filled with air at room pressure and coiled to a diameter of 30 cm. The cutback loss spectrum is shown in Fig. 1 and the experimentally measured losses are 0.007 dB/m at the pump wavelength, 0.005 dB/m at the first Stokes wavelength and 0.044 dB/m at the second Stokes wavelength. The actual fiber loss at the second Stokes wavelength is likely lower than measured value due to absorption from water in the air-filled fiber core. Figure 1 also shows the total absorption of methane as a function of wavelength over 1 m propagation distance held at 1 bar of pressure. The pump and first Stokes wavelengths experience minimal absorption, however several very closely spaced lines impact the second Stokes signal. The absorption due to the various lines varies from $\sim 20\%$ to near total absorption. While the gas absorption dominates the propagation losses at the second Stokes, the low loss design of the NANF allows for conversion of the pump to the first Stokes signal which in turn pumps the second Stokes signal.

2.2. Experimental setup

The experimental setup is shown in Fig. 2(a). The pump source used in this work is a Trumpf TruMicro 5050 disk laser. This laser produces 6 ps pulses with a repetition rate of 200 kHz centered at 1030 nm. The source can emit pulses with energy up to 250 μJ (average power of 50 W). The laser output is a linearly polarized and collimated beam with a diameter 5 mm. To couple the laser light into the fiber we utilize a three lens system. The first two lenses reduce the

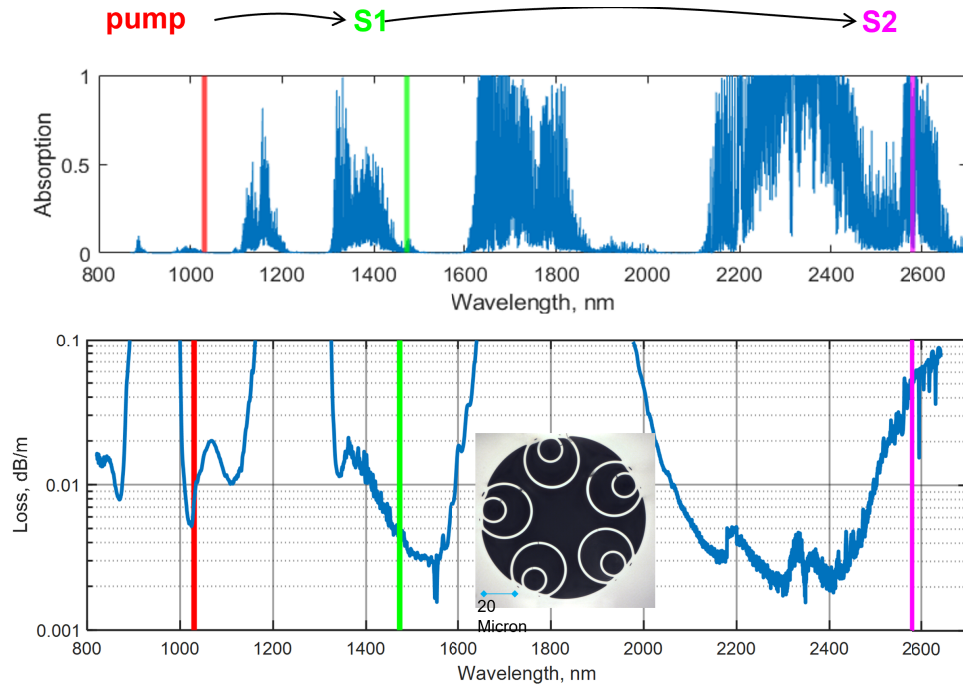


Fig. 1. Top: gas absorption of methane over a 1 m propagation path at 1 bar pressure as a function of wavelength. Bottom: Fiber loss as a function of wavelength with an SEM image of the custom NANF cross-section inset. Pump (1030 nm), first Stokes (~ 1472 nm), and second Stokes (~ 2580 nm) wavelengths are indicated by vertical lines.

diameter of the collimated beam and the third lens focuses the beam for coupling into the NANF. The focal lengths (specified in Fig. 2(a)) are chosen to result in an optimized beam diameter for coupling into the fundamental mode of the test fiber which has a mode field diameter of 28 μm . The coupling efficiency into the fiber is ~ 90%. The fiber under test is loosely coiled in a 30 – 40 cm diameter and the distal end of the fiber is held in a pressure interface where the filling gas is provided.

The output of the filled fiber passes through a magnesium fluoride window and a multi-port filter wheel (for filtering out the residual pump and first Stokes signals) terminating on a power meter. Silica and Indium Fluoride patch cables are positioned to capture optical scatter from the power meter and are connected to NIR and MIR OSAs as shown in 2(a). An image of an experiment in progress is shown in Fig. 2(c). The gas cell, CH₄ line, filter wheel, and fiber from Fig. 2(a) are visible in the photograph. The fiber is emitting visible red light, which comes from second anti-Stokes generation.

A pressure gradient will form along the fiber as one end of the fiber is held in a pressure interface while the other is open to the atmosphere. For a fiber of length L the pressure at location z is given by [31,32],

$$p(z) = \sqrt{p_0^2 - z(p_0^2 - p_L^2)/L} \quad (1)$$

where p_0 and p_L are the pressures at $z = 0$ and $z = L$ respectively. The steady state pressure gradient of varying fiber lengths with the distal end held at 4 bar is shown in Fig. 2(b). The exit cell is kept at a pressure set by the gas bottle regulator and the pressure gradient allowed to reach steady state before the experiment. We calculate the filling time required to reach steady state as being on the order of seconds by modelling the pressure driven flow in the fiber [33–35]. Once

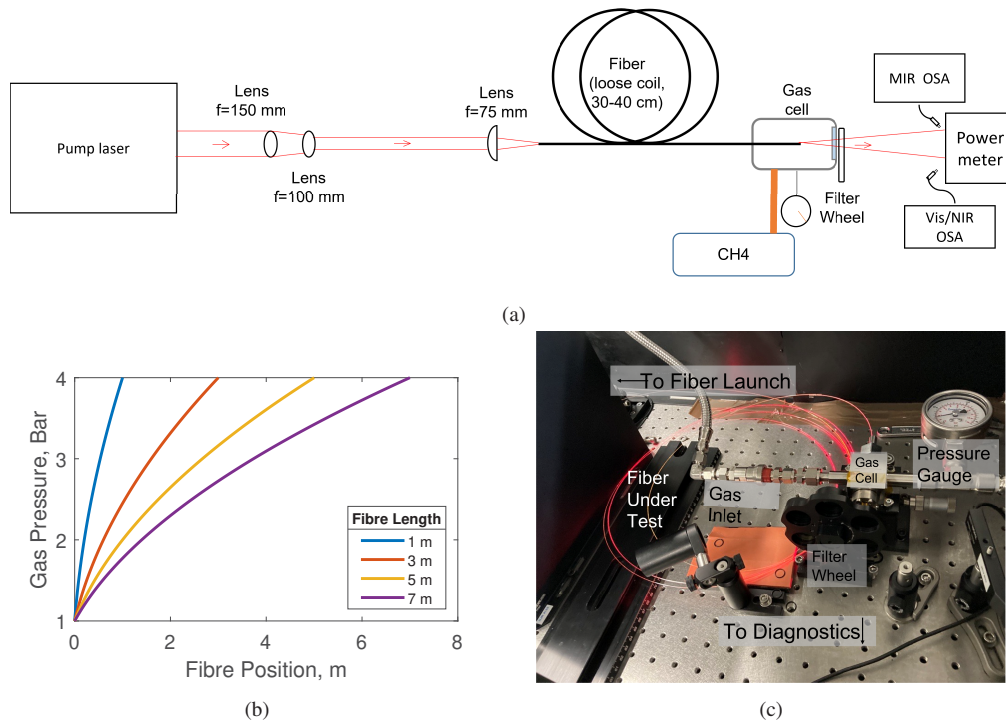


Fig. 2. Experimental setup: (a) block diagram, (b) steady state pressure gradient of various fiber length with the distal end held at 4 bar and (c) picture of a 515 cm fiber held at 2 bar pressure with 12 W launch power.

the pressure gradient is stable, spectra and power measurements are taken for each launch power. Spectra are taken when the beam passes through an empty filter port (i.e. no wavelengths are blocked). Power measurements are taken through an empty port as well as with long-pass filters with cut-on wavelengths at 1000 nm (to filter any potential anti-Stokes signals), 1300 nm (to isolate the first and second Stokes from the residual pump), and 1500 nm (to isolate the second Stokes). Figure 3 shows experimental spectra of a 160 cm length of fiber held at 3 bar. The first Stokes signal is generated immediately, it then levels off as the second Stokes signal begins to grow. In the experiment, discussed below, power and spectra are assessed for varying pressure (3 – 9 bar), launch power (1 – 15 W), and fiber length (125 – 585 cm) in order to maximize the second Stokes power.

2.3. Experimental results

It is known that net Raman gain may be increased by higher gas pressures and longer propagation lengths, but the gain increase is countered by loss due to infrared absorption of the methane gas. Therefore, fiber length and gas pressure are varied to maximize second Stokes output as a function of launch power. Initially a 135 cm length of fiber is filled with pressures varying from 3 – 9 bar. At each pressure, pump light of average power ranging from 1 – 15 W is coupled into the fiber and the power and spectra recorded in order to capture second Stokes power as a function of launch power. The results show an increased second Stokes power as pressure decreases and are shown in Fig. 4(a). The pressure which resulted in the greatest second Stokes power is 3 bar. The second Stokes power as a function of launch power of varying fiber lengths with a cell pressure of 3 bar is also assessed. Spectra and average power were recorded for a 5.85 m fiber for launch powers 1 – 15 W and the fiber is then cut to a shorter lengths and the process repeated

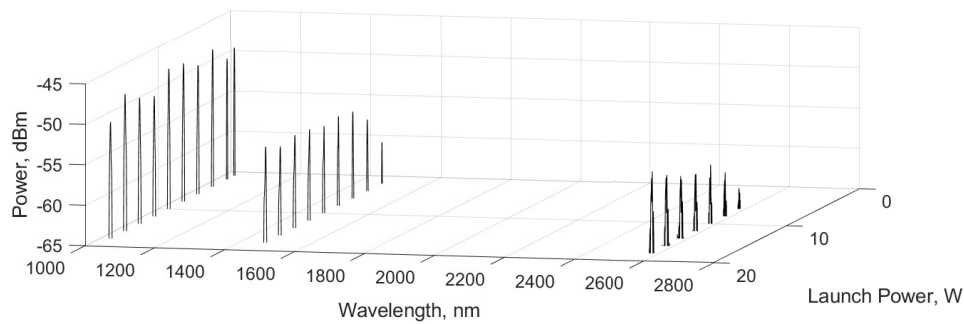


Fig. 3. Spectra showing the residual pump, first Stokes, and second Stokes signals at multiple launch powers.

each time to assess second Stokes power. For each reduced length the second Stokes power increases until the fiber is 125 cm in length, as shown in Fig. 4(b). While the long fibre lengths will have a greater net Raman gain, it also suffers from increased losses due to gas absorption. The second Stokes output is optimum at 160 cm, where it appears the loss-gain competition most favors second Stokes power output. Lengths shorter than 160 cm appear to have insufficient gain, resulting in both a higher threshold power and lower second Stokes output power. This process is repeated at 2 bar cell pressure and 160 cm resulted in the highest second stokes power. The optimum 160 cm length is subsequently assessed using pump powers of 1 – 36 W. The highest second Stokes output power achieved at 3 bar is 2.65 W and at 2 bar is 2.89 W as shown in Fig. 5(a). The experiment is truncated at 36 W launch power due to heating in the fiber coating. We believe the heating in the coating comes from multiple sources: quantum defect heating from the Raman process as well as absorption of the second Stokes signal due to methane infrared absorption. In practice the gas-pressure regulator used showed greater fluctuations when set to 1 bar than at higher pressures and so is not tested.

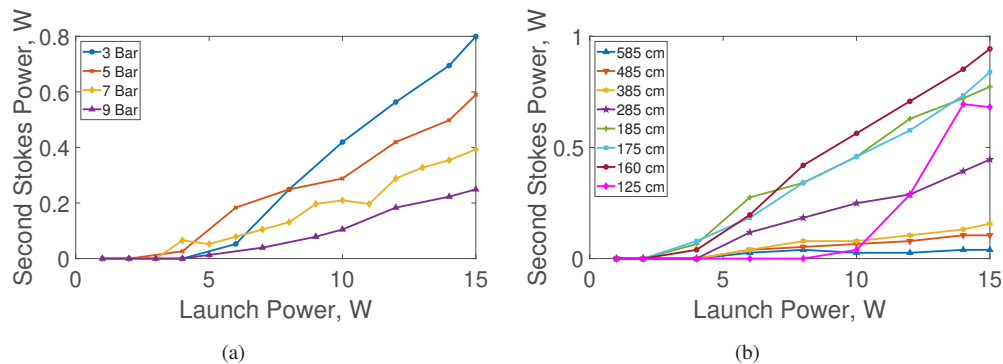


Fig. 4. (a) Second Stokes power through a 135 cm fiber at various pressures (b) Second Stokes power through various lengths of fiber at a gauge pressure of 3 bar.

Figure 5(b) shows the measured power of each of the Stokes signals normalized to the coupled launch power at 2 bar cell pressure. The first Stokes signal initially shows rapid growth with respect to the coupled launch power. This levels off as the second Stokes signal begins to grow. The depletion of the first Stokes signal becomes apparent by the drop at ~ 10 W launch power and the continued decrease until the final 36 W launch power. The proportion of the second Stokes signal power to coupled launch power continues to grow, but does not quite reach the level of the first Stokes. Given, the lack of saturation in the second Stokes signal measurement,

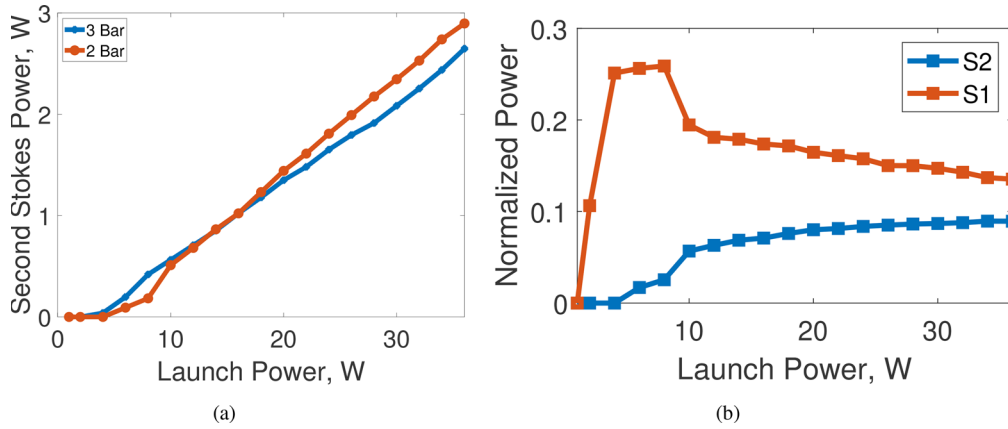


Fig. 5. (a) Second Stokes power through 160 cm of fiber at 2 and 3 bar gauge pressure, (b) Stokes signals normalized to coupled pump power with the cell pressure at 2 bar.

it is expected that increased launch power would continue to result in increased second Stokes power. In this experiment, the launch power is ultimately limited by heating in the fiber coating as stated above. Implementation of cooling along the length of the fiber may allow increased second Stokes power from increased launch power. As mentioned above, we did not test pressures lower than 2 bar however we expect that any improvements in the second Stokes signal power from lower pressures would be limited. We credit the clear increase in seconds Stokes signal power with decreasing pressure shown in Fig. 4(a) with a reduction in signal absorption at lower pressures, the improvement between cell pressures of 2 – 3 bar are less distinctive. This suggests we are very near the optimum balance of gain and loss to due to absorption.

We did not make a direct measurement of the 2580 nm signal, however we assume its duration is ~ 6 ps. As mentioned in section 1 the Stokes signals' pulse duration mirrors that of the pump source [16].

3. Modelling and simulation of methane filled NANF

Simple models of Raman generation, such as coupled differential equations, cannot be used here due to the complex time dynamics of working in the transient gain regime [29]. To reproduce experimental findings we employed the Generalized Nonlinear Schrodinger Equation (GNLSE) by adapting it to experimental conditions. The GNLSE is a well known, widely used model capable of capturing key interacting elements such as the chromatic dispersion and delayed molecular nonlinear effects. To the best of our knowledge, a GNLSE adapted to model methane has not been published in the literature yet. Here the GNLSE is formulated to include the loss, dispersion, and nonlinear properties of methane as well as the waveguiding properties of the fiber.

3.1. Model overview

The GNLSE is given as [29],

$$\frac{\partial \tilde{A}(z, \omega)}{\partial z} - iD(\omega)\tilde{A}(z, \omega) = i\gamma(\omega)\mathcal{F}\{A(z, T)\} \int_{-\infty}^{\infty} R(T')|A(z, T - T')|^2 dT' \quad (2)$$

where $\tilde{A}(z, \omega) = F(A(z, T))$ is the slowly evolving envelope of the electromagnetic field in the Fourier domain. The linear operator $D(\omega)$ includes both loss and dispersion, $D(\omega, p) = \beta(\omega, p) - \beta(\omega_0, p) - \beta_1(\omega_0, p)(\omega - \omega_0) + i\alpha(\omega, p)/2$. The frequency dependent propagation constant of the methane filled fiber at pressure p is $\beta(\omega, p)$ and $\beta_m(\omega_0, p)$ is the m th derivative

of β evaluated at the central propagation frequency and pressure p . All dispersion terms β_2 and higher are included in the simulation. This is accomplished by fitting the full propagation constant β to a polynomial and subtracting the constant and β_1 terms. The loss given by $\alpha(\omega, p)$ accounts for both waveguide propagation losses and pressure dependent infrared absorption of methane [36] as shown in Fig. 1. The right hand side of Eq. (2) gives the nonlinear response of the methane filled HCF to the propagating light and includes the instantaneous Kerr response and delayed Raman response. The nonlinear response is given by [37],

$$R(T) = (1 - f_r)\delta(T) + f_r H(T), \quad (3)$$

which includes both the instantaneous Kerr response as well as the delayed Raman response in $H(T)$. The fractional contribution of the Raman response to the total nonlinear response is given by f_r . To the best of our knowledge, no analytic model for the vibrational Raman response of methane exists. As has been done for other Raman active molecules, we instead model the Raman response as a simple damped oscillator [29,38],

$$H(T) = \frac{1 + T_2^2 \Omega_v^2}{T_2^2 \Omega_v} e^{-T/T_2} \sin(\Omega_v T) U(T), \quad (4)$$

where Ω_v is the Raman shift in Hz, T_2 is the dephasing time, and the Heaviside function $U(T)$ ensures causality [39].

3.2. Numerical simulation development and implementation

The GNLSE described above has been implemented successfully to describe pulse propagation through many materials. A successful implementation of the GNLSE relies heavily on accounting for experimental conditions in the modelling of the terms. Both the linear and nonlinear terms of the GNLSE for a gas-filled fiber are dependent on molecular density of the gas. This density is a function of both pressure and temperature. The Raman process generates heat and as mentioned in section 2.3 is a limiting factor for the work. The most substantial heating occurs over a length of a few centimeters as observed by a thermal camera, however the actual temperature of the gas remains unknown. While the implementation of a temperature gradient is preferable, given the unknown temperature and short propagation distance, the steady state pressure profile of a 160 cm length of the fiber under test is modelled using only Eq. (1). The impacts of changes in temperature on the generation remains an area of interest for future work.

The linear terms given by $D(\omega)$ in Eq. (2) are dispersion and loss. When operating away from waveguide resonances, the dispersive properties of HCF are well modelled by that of a capillary with the same core diameter [40]. The pump and Stokes signals do not propagate near the resonances allowing the use of the capillary approximation. The effective refractive index of the gas filled capillary is given as [41],

$$n(\lambda, P, T) = \sqrt{n_{\text{gas}}^2(\lambda, P, T) - \frac{2.404^2}{k^2 r^2}}, \quad (5)$$

where n_{gas} is the gas index of refraction determined from equations fit to experimental data for methane [42], k is the vacuum wave number, r is core radius, and the value 2.404 is the first zero of the first order Bessel function implying fundamental mode propagation. The propagation constant is given as $\beta = kn$ [37]. The sources of loss accounted for in α are waveguide loss as shown in Fig. 1 and methane infrared absorption as a function of both wavelength and gas pressure for the pressure gradient [36,43].

The nonlinear coefficient γ is a function of the nonlinear refractive index n_2 and is given as [37]

$$\gamma(\omega) = \frac{\omega_0 n_2}{c A_{eff}}, \quad n_2 = \frac{2\bar{n}_2}{\epsilon_0 n c}, \quad (6)$$

where ω is frequency, c is the speed of light, A_{eff} is the effective mode area of the fiber, ϵ_0 is the permittivity of vacuum, and n is the refractive index of the gas filled core. The nonlinear index coefficient is calculated from

$$\bar{n}_2 = \frac{3}{8n} \text{Re}(\chi^3), \quad (7)$$

where χ^3 is the third order nonlinear susceptibility [37]. In gases χ^3 is a pressure dependent value which can be determined from hyperpolarizability measurements for methane [44,45]. The fractional proportion of the nonlinear response to the Raman dynamic, f_r , is chosen to best fit the data. Within the Raman response function $H(T)$ the Raman dephasing time T_2 and the Raman shift Ω_v are unique to gas species and the values of T_2 and Ω_v are determined from spectroscopic data for methane. The dephasing time is inversely proportional to the Raman gain bandwidth in Hz [46], $\Delta\nu_g = (8220 + 377\rho) \times 10^6$ Hz [27],

$$T_2 = \frac{1}{\pi \Delta\nu_g} = \frac{1}{\pi(8220 + 377\rho) \times 10^6} \text{ s}, \quad (8)$$

where ρ is gas density in amagat. The Raman shift is the peak of the Raman gain spectrum for a given pressure and is given in cm^{-1} [47]

$$\Omega_v = 2916.72 - 0.169\rho. \quad (9)$$

Stokes signals build from optical noise which functions as a seed signal. To seed the Raman signals, quantum noise is included in the simulation. The noise used here is equivalent to one photon per mode at each frequency [37].

With the values of the pressure dependent terms calculated as a function of pressure from spectroscopic data, the f_r value is treated a free variable and varied to find the best match to the experimental data. For each f_r , the simulated first and second Stokes signals are compared to the experimentally obtained data from a 160 cm propagation at 3 bar cell pressure. To determine the best f_r , we compare: the growth rate of the Stokes signals relative to the launch power, the onset of the Stokes signals, as well as the Stokes signal widths. When the f_r value is too small the simulation overestimates the pump power needed to generate Stokes signals and underestimates the spectral width and growth rate of the Stokes signals. When the f_r value is too large it underestimates the pump power needed to generate the Stokes signal. It overestimates the growth and spectral width of the second Stokes signal and also prematurely predicts saturation of the second Stokes signal. When $f_r = 0.7$ the best match for Stokes onset, growth, and signal width is achieved. Figure 6 compares the experimental output of a 160 cm fiber with the pressure cell at 3 bar gauge pressure with $f_r = 0.7$. The simulation provides a good match both to the overall trend of the second Stokes growth (Figs. 6(a) and 6(b)) and individual spectra when compared to experiment (Figs. 6(c)–6(e)). In both the experimental and simulation results, the second Stokes signal spectrum exhibits a bifurcated structure and in the experimental results additional bands on the red side of the signal begin to form with increased launch power. We credit this structure to the methane absorption structure. While the generation of side bands is similar to that of a four-wave mixing process, the phase matching required is not satisfied here [29]. With a validated model for methane filled HCF, the GNLSE can be used for predicting behaviors in other experimental configurations. The GNLSE as formulated here would be of particular use for assessing performance across the transient gain regime and could capture the effects generated by pump sources in the femtosecond regime as well as longer picosecond duration pulses. Simulation of solitons and supercontinuum generation in methane filled HCF is also possible with this model.

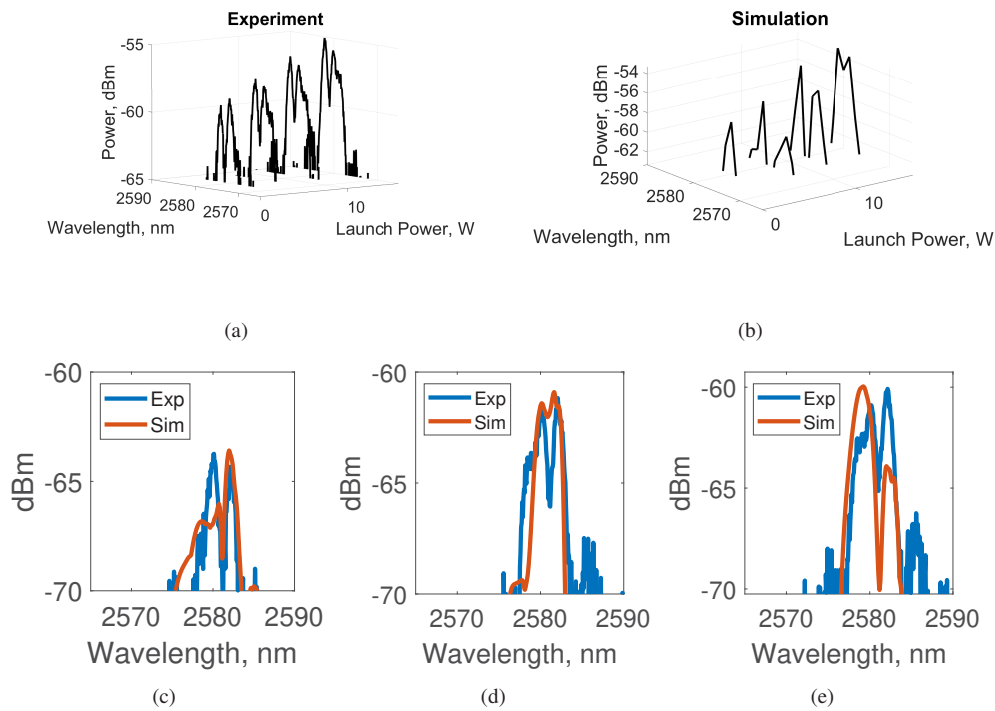


Fig. 6. (a) Experimental S2 spectra (b) Simulation S2 Spectra, and (c)-(e) are experimental and simulation spectra corresponding to a launch powers of (c) 4 W, (d) 6 W, (e) 8 W.

4. Summary and conclusions

In this work we have designed and fabricated a custom NANF with low-loss in three separate spectral regions to support a second-order vibrational Raman cascade in methane gas. The loss of the NANF is 0.007 dB/m at the pump wavelength, 0.005 dB/m at the first Stokes wavelength, and 0.044 dB/m at the second Stokes wavelength. The same fiber is used to achieve a 2.89 W, 2.58 μm , picosecond laser source via Raman cascade to the second Stokes wavelengths. To achieve this result, the interaction of Raman gain and power loss from infrared gas absorption were studied by varying propagation length and gas pressure to optimize the second Stokes power output. To the best of our knowledge, this result is the highest average power second Stokes cascade in a methane filled HCF to date, improving on the current state of the art by greater than a factor of ten [13], and the first at 2.58 μm .

To model the experimental results, we have used a single damped oscillator model of the methane molecule using previously published spectroscopic data. We have modelled the pressure gradient along the fiber to capture the impact of nonlinear effects (Raman gain, bandwidth, shift, and delay) and linear effects (infrared gas absorption and dispersion) in a GNLSE simulation. This model has been shown to match well the experimentally observed second Stokes growth trends and individual second Stokes spectra, opening a predictive space for modelling methane Raman interactions in the presence of a pressure gradient and losses due to gas absorption.

Funding. Engineering and Physical Sciences Research Council, Airguide (EP/P030181/1).

Disclosures. The authors declare no conflict of interest.

Data availability. Data underlying the results presented in this paper are available in the University of Southampton Repository.

References

1. C. R. Petersen, U. Möller, I. Kubat, B. Zhou, S. Dupont, J. Ramsay, T. Benson, S. Sujecki, N. Abdel-Moneim, Z. Tang, D. Furniss, A. Seddon, and O. Bang, "Mid-infrared supercontinuum covering the 1.4–13.3 micron molecular fingerprint region using ultra-high NA chalcogenide step-index fibre," *Nat. Photonics* **8**(11), 830–834 (2014).
2. M. W. Sigrist, "Mid-infrared laser-spectroscopic sensing of chemical species," *J. Adv. Res.* **6**(3), 529–533 (2015).
3. R. Knappe, H. Haloui, A. Seifert, A. Weis, and A. Nebel, "Scaling ablation rates for picosecond lasers using burst micromachining," in *SPIE LASE: Laser-based Micro- and Nanopackaging and Assembly IV*, vol. 7585 (2010), pp. 75850H 1–6.
4. A. Urich, R. R. J. Maier, F. Yu, J. C. Knight, D. P. Hand, and J. D. Shephard, "Flexible delivery of Er:YAG radiation at 294 μm with negative curvature silica glass fibers: a new solution for minimally invasive surgical procedures," *Biomed. Opt. Express* **4**(2), 193–205 (2013).
5. A. B. Seddon, T. M. Benson, S. Sujecki, *et al.*, "Towards the mid-infrared optical biopsy," in *Proceedings of SPIE: Optical Biopsy XIV*, vol. 9703 (San Francisco CA, US, 2016), p. 970302.
6. K. N. Bourdakos, L. Xu, A. Crisford, D. Xu, I. Abughazaleh, P. B. Johnson, H. Cook, P. Srisamran, R. O. C. Oreffo, D. J. Richardson, and S. Mahajan, "Deep tissue imaging with multiphoton microscopy in the short-wavelength infrared windows," in *Frontiers in Biophotonics and Imaging II*, vol. 12333 S. Mahajan, ed., International Society for Optics and Photonics (SPIE, 2023), p. 123330E.
7. Y. Su, W. Wang, X. Hu, H. Hu, X. Huang, Y. Wang, J. Si, X. Xie, B. Han, H. Feng, Q. Hao, G. Zhu, T. Duan, and W. Zhao, "10 Gbps DPSK transmission over free-space link in the mid-infrared," *Opt. Express* **26**(26), 34515–34528 (2018).
8. A. I. Adamu, M. S. Habib, C. R. Petersen, J. E. A. Lopez, B. Zhou, A. Schülzgen, M. Bache, R. Amezcua-Correa, O. Bang, and C. Markos, "Deep-UV to Mid-IR Supercontinuum Generation driven by Mid-IR Ultrashort Pulses in a Gas-filled Hollow-core Fiber," *Sci. Rep.* **9**(1), 4446 (2019).
9. N. Akhmediev and W. Chang, "Mid-infrared supercontinuum generation in supercritical xenon-filled hollow-core negative curvature fibers," *Opt. Lett.* **41**(21), 5122–5125 (2016).
10. F. Benabid, J. C. Knight, G. Antonopoulos, and P. S. J. Russell, "Stimulated Raman scattering in hydrogen-filled hollow-core photonic crystal fiber," *Science* **298**(5592), 399–402 (2002).
11. F. Benabid, G. Bouwmans, J. C. Knight, P. J. St Russell, and F. Couny, "Ultrahigh Efficiency Laser Wavelength Conversion in a Gas-Filled Hollow Core Photonic Crystal Fiber by Pure Stimulated Rotational Raman Scattering in Molecular Hydrogen," *Phys. Rev. Lett.* **93**(12), 123903 (2004).
12. M. Cassataro, D. Novoa, M. C. Günendi, N. N. Edavalath, M. H. Frosz, J. C. Travers, and P. S. Russell, "Generation of broadband mid-IR and UV light in gas-filled single-ring hollow-core PCF," *Opt. Express* **25**(7), 7637–7644 (2017).
13. L. Cao, S.-f. Gao, Z.-g. Peng, X.-c. Wang, Y.-y. Wang, and P. Wang, "High peak power 2.8 μm Raman laser in a methane-filled negative-curvature fiber," *Opt. Express* **26**(5), 5609–5615 (2018).
14. Y. Chen, Z. Wang, B. Gu, F. Yu, and Q. Lu, "Achieving a 1.5 micrometer fiber gas Raman laser source with about 400 kW of peak power and a 63 GHz linewidth," *Opt. Lett.* **41**(21), 5118–5121 (2016).
15. Y. Chen, Z. Wang, Z. Li, W. Huang, X. Xi, and Q. Lu, "Ultra-efficient Raman amplifier in methane-filled hollow-core fiber operating at 1.5 μm ," *Opt. Express* **25**(17), 20944–20949 (2017).
16. Y. Chen, Z. Wang, N. Zhang, and Q. Lu, "Spectral characteristics of CH₄-filled hollow-core fiber Raman laser amplifier," in *ICOCN 2017 - 16th International Conference on Optical Communications and Networks*, (Institute of Electrical and Electronics Engineers Inc., 2017).
17. S. Edelstein and A. A. Ishaaya, "Efficient raman conversion in sf₆- and cf₄-filled hollow-core photonic bandgap fibers," in *Conference on Lasers and Electro-Optics*, (Optica Publishing Group, 2020), p. JTu2F.36.
18. S. F. Gao, Y. Y. Wang, F. Belli, C. Brahm, P. Wang, and J. C. Travers, "From Raman Frequency Combs to Supercontinuum Generation in Nitrogen-Filled Hollow-Core Anti-Resonant Fiber," *Laser Photonics Rev.* **16**(4), 2100426 (2022).
19. A. V. Gladyshev, A. F. Kosolapov, A. N. Kolyadin, M. S. Astapovich, A. D. Pryamikov, M. E. Likhachev, and I. A. Bufetov, "Mid-IR hollow-core silica fibre Raman lasers," *Quantum Electron.* **47**(12), 1078–1082 (2017).
20. A. V. Gladyshev, A. N. Kolyadin, A. F. Kosolapov, Y. P. Yatsenko, A. D. Pryamikov, A. S. Biriukov, I. A. Bufetov, and E. M. Dianov, "Low-threshold 1.9 μm Raman generation in microstructured hydrogen-filled hollow-core revolver fibre with nested capillaries," *Laser Phys.* **27**(2), 025101 (2017).
21. A. V. Gladyshev, M. S. Astapovich, Y. P. Yatsenko, A. F. Kosolapov, A. G. Okhrimchuk, and I. A. Bufetov, "SRS generation of femtosecond pulses in a methane-filled revolver hollow-core optical fibre," *Quantum Electron.* **49**(12), 1089–1092 (2019).
22. N. Kotsina, F. Belli, S. F. Gao, Y. Y. Wang, P. Wang, J. C. Travers, and D. Townsend, "Ultrafast molecular spectroscopy using a hollow-core photonic crystal fiber light source," *J. Phys. Chem. Lett.* **10**(4), 715–720 (2019).
23. Z. Wang, Z. Li, W. Huang, and Y. Cui, "Efficient cascade Raman source in methane-filled hollow-core fibers operating at 2.8 μm ," in *SPIE/COS Photonics Asia*, (SPIE-Intl Soc Optical Eng, Beijing, China, 2018), p. 24.
24. G. T. Jasion, H. Sakr, J. R. Hayes, S. R. Sandoghchi, L. Hooper, E. N. Fokoua, A. Saljoghei, H. C. Mulvad, M. Alonso, A. Taranta, T. D. Bradley, I. A. Davidson, Y. Chen, D. J. Richardson, and F. Poletti, "0.174 db/km hollow core double nested antiresonant nodeless fiber (dnanf)," in *2022 Optical Fiber Communications Conference and Exhibition (OFC)*, (2022), pp. 1–3.
25. F. Poletti, "Nested antiresonant nodeless hollow core fiber," *Opt. Express* **22**(20), 23807 (2014).

26. W. Huang, Z. Wang, Z. Zhou, W. Pei, Y. Cui, X. Li, Z. Li, and J. Chen, "Tunable fiber gas raman laser of 6 w at 2.9 micron by deuterium-filled hollow-core fiber," *IEEE Journal of Selected Topics in Quantum Electronics* **Early Access**, 1–7 (2023).
27. M. Weber, *Handbook of Optical Materials* (CRC Press LLC, 2003).
28. H. Haken and H. C. Wolf, *Molecular Physics and Elements of Quantum Chemistry* (Springer-Verlag, Berlin, Germany, 1995), 1st ed.
29. S. A. Mousavi, H. C. H. Mulvad, N. V. Wheeler, P. Horak, J. Hayes, Y. Chen, T. D. Bradley, S.-u. Alam, S. R. Sandoghchi, E. N. Fokoua, D. J. Richardson, and F. Poletti, "Nonlinear dynamic of picosecond pulse propagation in atmospheric air-filled hollow core fibers," *Opt. Express* **26**(7), 8866–8882 (2018).
30. F. Couny, O. Carraz, and F. Benabid, "Control of transient regime of stimulated Raman scattering using hollow-core PCF," *J. Opt. Soc. Am. B* **26**(6), 1209–1215 (2009).
31. C. Markos, J. C. Travers, A. Abdolvand, B. J. Eggleton, and O. Bang, "Hybrid photonic-crystal fiber," *Rev. Mod. Phys.* **89**(4), 045003 (2017).
32. R. Pennetta, M. Enders, M. Frosz, F. Tani, and P. Russell, "Fabrication and non-destructive characterization of tapered single-ring hollow-core photonic crystal fiber," *APL Photonics* **4**(5), 056105 (2019).
33. S. Rikimi, Y. Chen, T. W. Kelly, I. A. Davidson, G. T. Jasion, M. Partridge, K. Harrington, T. D. Bradley, A. A. Taranta, F. Poletti, M. N. Petrovich, D. J. Richardson, and N. V. Wheeler, "Internal Gas Composition and Pressure in As-drawn Hollow Core Optical Fibers," *J. Lightwave Technol.* **40**(14), 4776–4785 (2022).
34. B. M. Masum, S. M. Aminossadati, M. S. Kizil, and C. R. Leonardi, "Numerical and experimental investigations of pressure-driven gas flow in hollow-core photonic crystal fibers," *Appl. Opt.* **58**(4), 963 (2019).
35. E. Elistratova, T. W. Kelly, I. A. Davidson, H. Sakr, T. D. Bradley, A. Taranta, F. Poletti, R. Slavík, P. Horak, and N. V. Wheeler, "Distributed Measurement of Hollow-Core Fibre Gas Filling and Venting via Optical Time-Domain Reflectometry," in *Distributed Measurement of Hollow-Core Fibre Gas Filling and Venting via Optical Time-Domain Reflectometry*, vol. 4776 (CLEO Europe 2023, 2023), p. 1.
36. Y. Babikov, "HiTran on the Web," <https://hitran.iao.ru/home> (2023).
37. G. P. Agrawal, *Nonlinear Fiber Optics* (Academic Press, 2007), 5th ed.
38. Q. Lin and G. P. Agrawal, "Raman response function for silica fibers," *Opt. Lett.* **31**(21), 3086–3088 (2006).
39. K. J. Blow and D. Wood, "Theoretical Description of Transient Stimulated Raman Scattering in Optical Fibers," *IEEE J. Quantum Electron.* **25**(12), 2665–2673 (1989).
40. M. A. Finger, N. Y. Joly, T. Weiss, and P. S. Russell, "Accuracy of the capillary approximation for gas-filled kagomé-style photonic crystal fibers," *Opt. Lett.* **39**(4), 821–824 (2014).
41. J. C. Travers, W. Chang, J. Nold, N. Y. Joly, P. St. J. Russell, and P. J. St Russell, "Ultrafast nonlinear optics in gas-filled hollow-core photonic crystal fibers [Invited]," *J. Opt. Soc. Am. B* **28**(12), A11–A26 (2011).
42. R. Rollefson and R. Havens, "Index of refraction of methane in the infra-red and the dipole moment of the CH bond," *Phys. Rev.* **57**(8), 710–717 (1940).
43. L. R. Brown, D. C. Benner, J. P. Champion, *et al.*, "Methane line parameters in HITRAN," *J. Quant. Spectrosc. Radiat. Transfer* **82**(1-4), 219–238 (2003).
44. H. J. Lehmeier, W. Leupacher, and A. Penzkofer, "Nonresonant third order hyperpolarizability of rare gases and N₂ determined by third harmonic generation," *Opt. Commun.* **56**(1), 67–72 (1985).
45. D. P. Shelton, "Nonlinear-optical susceptibilities of gases measured at 1064 and 1319nm," *Phys. Rev. A* **42**(5), 2578–2592 (1990).
46. M. G. Raymer and J. Mostowski, "Stimulated Raman scattering: Unified treatment of spontaneous initiation and spatial propagation," *Phys. Rev. A* **24**(4), 1980–1993 (1981).
47. R. Lopert, "Measured Stimulated Raman Gain in Methane," Ph.D. thesis, University of California, Davis (1983).